Earth Systems and Environment (2019) 3:189–202
https://doi.org/10.1007/s41748-019-00103-2

ORIGINAL ARTICLE

On the Influence of Variations in Solar Irradiance on Climate: A Case Study of West Africa

Mojisola Oluwayemisi Adeniyi[1]

Received: 14 November 2018 / Accepted: 11 June 2019 / Published online: 18 June 2019

Abstract
Variations in total solar irradiance (TSI) are known to affect the climate, but the extent at specific locations on the globe is not known. This paper uses the version 4.7 of the regional climate model (RegCM4.7) developed at the International Centre for Theoretical Physics to simulate the influence of ± 5 W m^{-2} changes in TSI on the precipitation, temperature, evapotranspiration, water availability for plant, and heat stress over West Africa. In general, the 5 W m^{-2} increase in TSI results in increase in precipitation, temperature, evapotranspiration, water availability for plants, and heat stress, while reduction of 5 W m^{-2} in TSI reduces the magnitude of the variables. It results in increase in irrigation water need. However, the induced changes are latitudinal. Latitudes 15–25°N stand out in the TSI ± 5 W m^{-2} experiments for contrary-induced changes in near-surface air temperature with respect to the induced changes in the whole domain. This is attributed to the cooling associated with evaporation increase due to TSI increase and vice versa.

Keywords Solar irradiance · Meridional moisture flux · Discomfort index · Regional climate model · West Africa

1 Introduction

Every natural activity on earth derives its energy from the sun; plants would not undergo photosynthesis unless a substantial energy is received from the sun (Montheith and Unsworth 2013; Adeniyi et al. 2012). The subsequent energy derived from photosynthesis has important implications for food productivity, species, and life sustenance in general (Bassham and Hans 2018). The economy of some West African countries depends on the energy from photosynthesis in form of fossil fuels (Bassham and Hans 2018). The atmospheric circulation is also powered by the sun (Adeniyi and Oyekola 2017; Guo et al. 2018). Greenhouse gases have played a major role in the on-going warming of the global atmosphere (Zhang et al. 2013; Zaehle et al. 2011). However, greenhouse gases have no job without the short-wave solar irradiance which warms the earth before the subsequent release of the energy in the infrared region into the atmosphere and absorption by greenhouse gases.

Changes in total solar irradiance (TSI) during total solar eclipse have been shown to affect the weather (Nymphas et al. 2009); such a change is almost a power shutdown from the sun for only a few minutes. This affects other meteorological parameters on the day of solar eclipse occurrence. This type of change is abrupt and does not occur often in a particular location; however, about two-to-four solar eclipses occur in a year (Lithman and Espenak 2017; Espenak 1989) and are seen in some places around the globe.

The TSI varies (Yeo et al. 2014; Kopp 2016), and it has varied from 1360 to 1375 W m^{-2} within the period 1978–2013 depending on the satellite data (Yeo et al. 2014; Kopp 2016). This is a difference of about 15 W m^{-2}. However, the changes are not usually abrupt, but follow a cycle. It is clear that changes in the solar constant will affect the climate (Wild 2009), but the extent and nature of the effect in specific locations is not known. Regional climate models usually replicate observations better due to their relatively fine resolution and topographical representation of the surface (Gao et al. 2016), so they have been used extensively in regional climate studies (Miguez-Macho et al. 2005; Rojas 2006; Giorgi et al. 2012; Adeniyi 2014; Coppola et al. 2014; Gao et al. 2016; Adeniyi 2017). This paper uses the version 4.7 of the regional climate model (RegCM4.7.0) developed at International Centre for Theoretical Physics to examine

✉ Mojisola Oluwayemisi Adeniyi
mojisolaadeniyi@yahoo.com

[1] Department of Physics, University of Ibadan, Ibadan, Nigeria

how the climate would be affected with ± 5 W m^{-2} changes in TSI based on an idealised concept. The previous versions of RegCM4 have been used to simulate the climate over West Africa (Giorgi et al. 2012; Adeniyi 2014, 2017; Coppola et al. 2014) with moderate skill.

2 Model Setup

Three sets of simulations are done using the hydrostatic core of RegCM4.7.0 developed at the International Centre for Theoretical Physics, Trieste, Italy. One served as the control simulation with TSI value of 1367 W m^{-2}, while the other two use TSI of $1367+5$ W m^{-2} and $1367-5$ W m^{-2}. The three experiments use the same set of model physics and parameterizations. The simulations are done on 0.5×0.5 degree grids with 23 vertical levels over West Africa. The domain has 120×120 grid points centred on longitude 0°E and latitude 20°N. The domain cartographic projection, model physics, and parameterization schemes used in this study are similar to the ones used in Adeniyi (2017) with a few exceptions which are listed in Table 1. All the simulations start from 01 Jan 2004 and end at 01 Jan 2009, and the last 4 years are analysed to allow for spin-up time and model stability.

3 Data and Methodology

3.1 Evaluation Data

The ability of Tiedtke CPPS on land and Kain–Fritsch CPPS on ocean in RegCM4.7.0 to simulate diurnal and monthly precipitation is evaluated using Tropical Rainfall Measuring Mission (TRMM_3B42) 3 hourly precipitation data (Huffman et al. 2007), University of Delaware Precipitation and Air Temperature v4.01 (UDEL, Legates and Willmott 1990; Willmott and Matsuura 1995, 2001), and Climate Research Unit (CRU TS3.24.01) monthly precipitation data (Harris et al. 2014). Temperature simulation in RegCM4.7 is also compared with UDEL and CRU monthly temperature observations.

The TRMM_3B42 on 0.25×0.25 degrees grid is an optimally adjusted infrared brightness temperature estimates based on combined 2B-31, 2A-12, SSMI, AMSR, and AMSU satellite estimated precipitation data. The calibration algorithm is described in detail in http://trmm.gsfc.nasa.gov/3b42.html.

CRU time series are gridded data on 0.5×0.5 degrees grid developed from station data (Harris et al. 2014). The UDEL data are also station-based (Legates and Willmott 1990; Willmott and Matsuura 1995, 2001).

3.2 Vertically Integrated Meridional Moisture Flux

Vertically integrated meridional moisture flux is calculated for each grid in the simulation domain based on Eq. (1) (Soares and Marengo 2009; Tsukernik and Lynch 2013):

Vertically integrated meridional moisture flux

$$= -\int_{p1}^{p2} \frac{(\text{hus} \times \text{va})}{\text{g}} \times \text{dp}, \tag{1}$$

where hus is the mean seasonal specific humidity, va is the mean seasonal meridional wind speed, $p1=1000$, $p2=300$, and $\text{dp}=300–1000$.

3.3 Discomfort Index

The discomfort index (DI) is computed based on Kibler (1964) formulation used in Adeniyi (2009) given by Eq. (2). The index uses temperature and relative humidity:

$$\text{DI} = (1.8\times\text{tas}) + 32 - ((1-\text{hurs})\times(\text{tas}-14.3)), \tag{2}$$

where tas is the mean seasonal near-surface temperature and hurs is the mean seasonal near-surface relative humidity as a fraction.

Temperature humidity index (THI) of Kibler (1964) is old, but the relationship between heat stress, temperature, and relative humidity remains valid. This index was developed at Missouri in USA. Thom (1959) THI was also developed in USA at the Office of Climatology, US Weather

Table 1 Additional parameterizations and boundary condition used in this study

Quasimonotonic semilagragian scheme	Bermejo and Staniforth (1992)
Convective precipitation parameterization scheme	
(CPPS) on land	Tiedtke (1996)
CPPS on ocean	Kain and Fritsch (1990) and Kain (2004)
Lake model	Hostetler et al. (1993)
Initial and lateral boundary condition	Era interim reanalysis (ERAIN75) (Dee et al. 2011)
Oceanic boundary condition	ERAIN75
Soil moisture initialization	European Space Agency—climate change initiative (ESA-CCI) data

Bureau. Thom (1959) and Kibler (1964) THI usually give almost the same index values with correlation of 1.0 (Okpara et al. 2002; Adeniyi 2009). The index has been widely used; it was applied in Tunisia (Ben Salem and Bouraoui 2009), Southern Africa (Du Preez et al. 1990), Mediterranean in Croatia (Gantner et al. 2011), and in West Africa (Okpara et al. 2002). Okpara et al. (2002) applied Thom (1959) and Kibler (1964) THI to study heat stress impact on people at Akure.

The scale for significance of THI is adopted from Thom (1959) and validated using response of cattle milk yield to heat stress in Nigeria based on the published milk yield in Chafa (2015). When DI value is greater than 80, the weather is uncomfortable to all animals and man, when $75 \le DI \le 80$; half of the population is uncomfortable because of high humidity and hot weather. With $65 \le DI \le 75$, the whole population is comfortable. With $60 \le DI \le 65$, half of the population is partially comfortable, while the remaining halves are uncomfortable due to low humidity and cold. When DI value is less than 60, the whole population is uncomfortable due to unbearable cold and dry weather.

4 Results and Discussion

4.1 Simulation of Diurnal Precipitation

The domain of simulation is shown in Fig. 1. It comprises of West Africa and extends to northern Africa, Mediterranean sea, southern Spain, southern Italy, and Greece. The five boxes within the domain are predefined regions of precipitation in Adeniyi (2016). Their area averages for diurnal precipitation and monthly precipitation and temperature observation climatology are compared with simulation for model evaluation.

Area average of mean 3 hourly precipitation from 2005 to 2008 over each region of precipitation in simulation is compared with TRMM observation for the same period in Fig. 2. At WWA, between midnight 00 and 09 h (before noon), RegCM4.7 underestimates the diurnal rainfall rate (mm h^{-1}) and overestimates it between 09 and 18 h (Fig. 2a). The diurnal trend is fairly captured between noon and 18 h. However, there is bias with a maximum value of 0.14 mm h^{-1}. The diurnal trend is fairly captured at CGC also with bias ranging from 0.1 to 0.19 mm h^{-1} (Fig. 2b). At EGC, the diurnal trend is moderately captured with large biases from 15 to 06 h (Fig. 2c). The diurnal peaks at ES are not well simulated by RegCM4.7, but the bias is low from 06 to 18 h (Fig. 2d). From 00 to 18 h, the trend of diurnal precipitation at LES is well captured with bias ranging from 0 to 0.12 mm h$^{-1.}$

4.2 Simulation of Monthly Precipitation

The two observational data sets agree on the peak periods and intra-annual variations with small variance except at EGC and ES where there is more bias. Monthly precipitation is well simulated at WWA with little overestimation and the peak period is well captured (Fig. 3a). The peak period is well simulated at ES but with high negative bias (Fig. 3d) throughout the year with the exception of March and April when there is overestimation. The two observational data only agree on the peak period and rainfall peak value in this region (ES), they are at variance from May to July and from September to November. At LES, two peaks

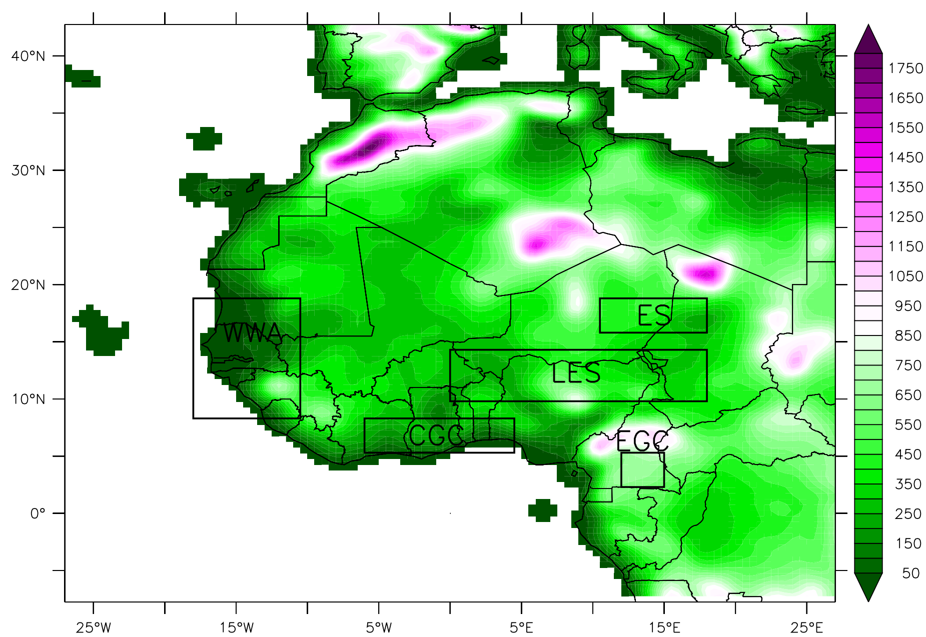

Fig. 1 Topography of the simulation domain and predefined regions of precipitation over West Africa (Adeniyi 2016)

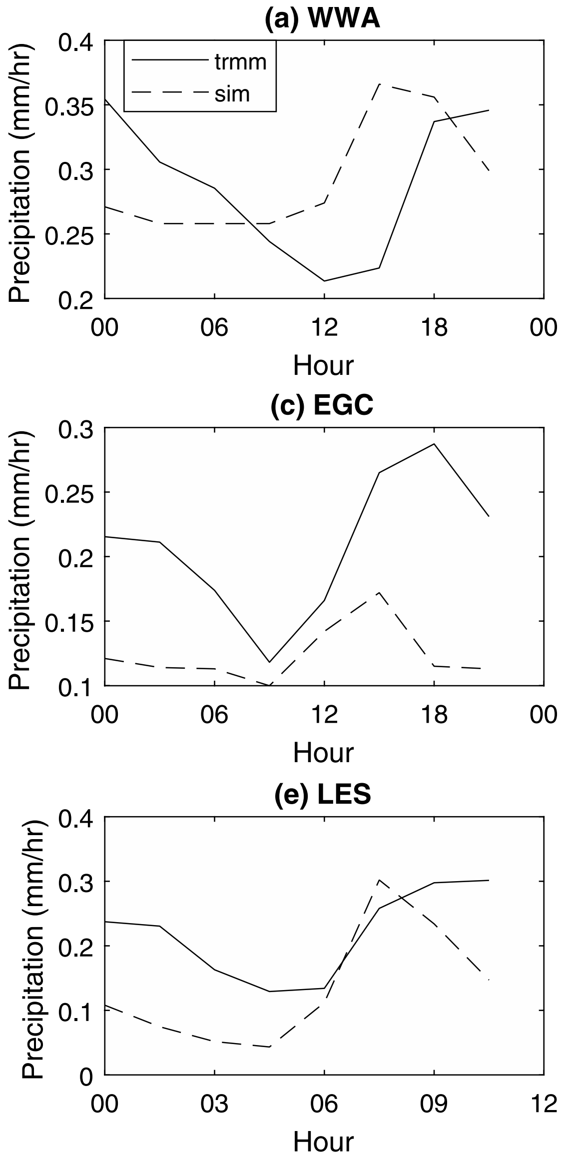

Fig. 2 Mean JJAS diurnal precipitation from TRMM observation and control simulation in five precipitation regions over West Africa

are simulated against only one peak in observation with overestimation from January to May. The second peak in August matches with the only peak in observation with negative bias (Fig. 3d). At CGC and EGC, the two peaks in observation are simulated at little variance to observation with negative bias between July and September at CGC and between August and October at EGC. Overestimation of mean monthly precipitation prevails in the remaining months of the year. The observed little dry season at CGC in August (Akisanola et al. 2016) is captured by both CRU and UDEL. At EGC, the little dry season is observed in July; the model simulates the little dry season from June to September. The model has the best performance in simulating intra-annual precipitation variations at WWA followed by EGC and CGC. The model performance at the Sahel is not so good.

4.3 Simulation of Intra-annual Temperature Variation

Figure 4 compares intra-annual temperature variations in observations and simulation in five regions over West Africa. CRU and UDEL observations agree on intra-annual temperature variations in all the regions considered except for higher bias in August and October at ES. RegCM4.7 underestimates temperature in all the regions with least bias

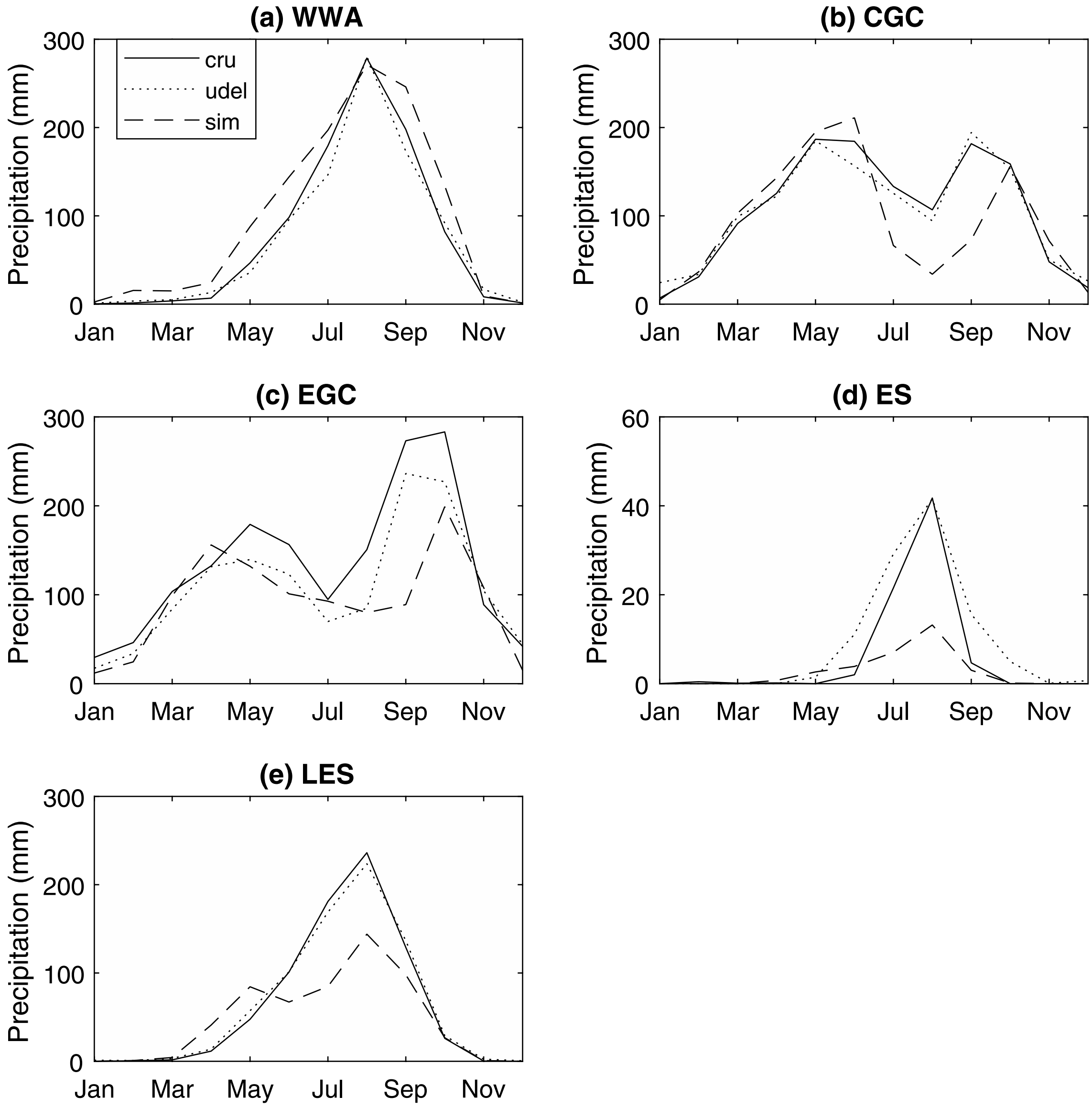

Fig. 3 Monthly climatology of precipitation from observations (CRU and UDEL) and control simulation in five precipitation regions over West Africa

at EGC, followed by CGC, ES, LES, and WWA. However, the peak periods are well simulated in all the regions. The previous versions of RegCM4 have been reported to underestimate temperature (Adeniyi 2014, 2017).

4.4 Induced Changes in Mean Seasonal Precipitation

Figure 5 shows the simulated induced changes in mean seasonal (June–September, JJAS) precipitation in response to ± 5 W m^{-2} changes in TSI over the domain of simulation. With + 5 W m^{-2} change, it is expected that temperature and precipitation should increase everywhere in the domain, all things being equal. Due to the expected increase in evaporation and convection, that should increase rainfall amount on the long run. Figure 5d reveals little or no change beyond latitude 15°N on land with the exception of Morocco. The southern countries in the domain show some precipitation increase as expected. On the ocean, there is little or no change which tends towards precipitation reduction. For 5 W m^{-2} reduction in TSI, precipitation reduces with noticeable changes only at the southern countries in the domain (Fig. 5e). The increase in precipitation with increase in TSI can be attributed to increase in evaporation and transpiration at the surface of water bodies and vegetation due to increased solar irradiance which can support convection and cloud development that can precipitate on the land areas. On the other hand,

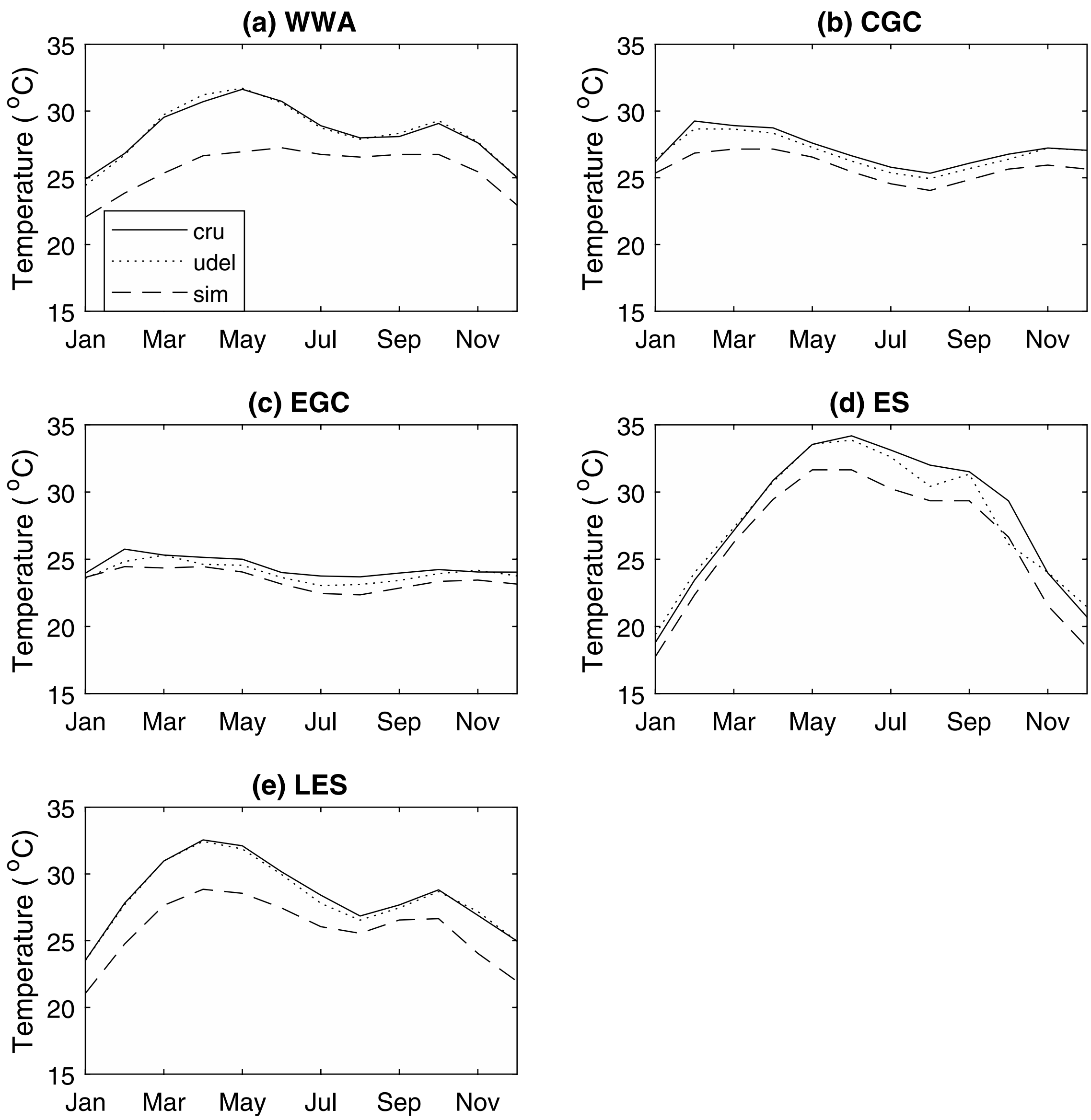

Fig. 4 Monthly climatology of temperature from observations (CRU and UDEL) and control simulation in five precipitation regions over West Africa

reduction in TSI reduces the input for evaporation that can aid cloud development and subsequent rainfall over the domain.

4.5 Induced Changes in Mean Seasonal Temperature

Changes in near-surface air temperature based on TSI changes are shown in Fig. 6. Temperature changes in response to ± 5 W m^{-2} changes in TSI over the domain of simulation are latitudinal-dependent. Increase in temperature is expected all over the simulation domain based on $+5$ W m^{-2} TSI increase, since solar irradiance should increase. Figure 6d shows a general increase in temperature over both ocean and land except for the latitudes 15–25°N where cooling prevails. The cooling is probably due to the evaporation increase (Philander 1998) in the area due to increased TSI which eventually leads to cooling in the area. Some southern countries also show some degree of cooling. In response to 5 W m^{-2} TSI reduction, Fig. 6e shows a general reduction in near-surface air temperature over the ocean and south eastern part of the domain. Patches of temperature

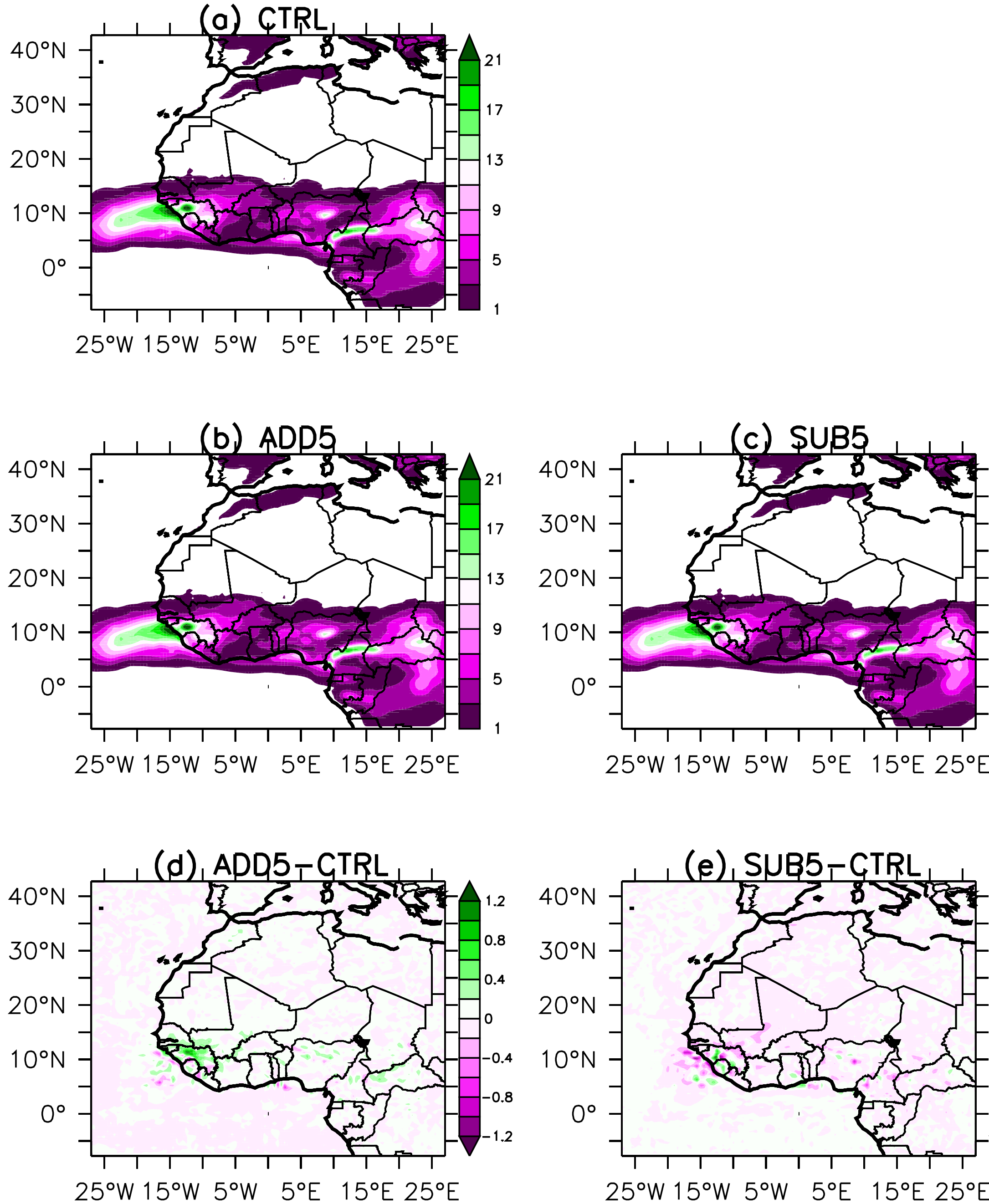

Fig. 5 Induced changes in precipitation based on increase or reduction of 5 W m^{-2} in solar constant. **a** Mean JJAS precipitation from control simulation, **b** mean JJAS precipitation from 5 W m^{-2} increase in solar constant simulation, **c** mean JJAS precipitation from 5 W m^{-2} reduction in solar constant simulation, **d** difference between (**b**) and (**a**), and **e** difference between (**c**) and (**a**)

reduction are located at the northern countries. However, there is pronounced warming between 15 and 25°N over Mali and Niger where cooling prevails in the TSI + 5 W m^{-2} experiment. The warming here instead of general cooling could be explained based on reduced evaporation that follows reduction in TSI. Instead of cooling, the resultant consequence is warming in the area.

4.6 Induced Changes in Integrated Meridional Moisture Flux and Evapotranspiration

Figure 7 shows vertically integrated meridional moisture flux from 1000 to 300 hPa. Vertically integrated meridional moisture flux generally increases on land in response to TSI increase, except for some few locations at the north (Fig. 7d). In the TSI − 5 W m^{-2} experiment,

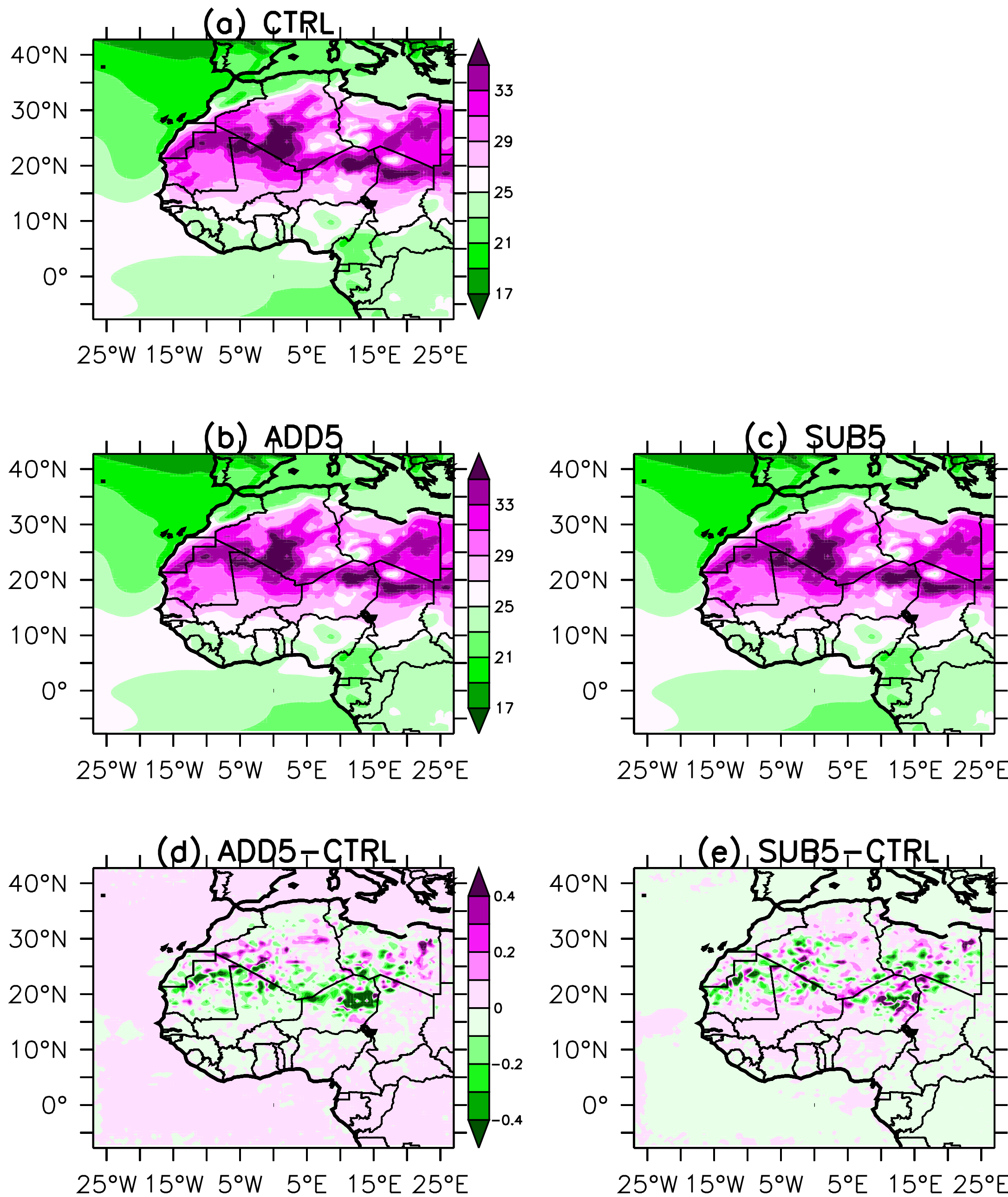

Fig. 6 Induced changes in near-surface air temperature based on increase or reduction of 5 W m^{-2} in solar constant. **a** Mean JJAS temperature from control simulation, **b** mean JJAS temperature from 5 W m^{-2} increase in solar constant simulation, **c** mean JJAS temperature from 5 W m^{-2} reduction in solar constant simulation, **d** difference between (**b**) and (**a**), and **e** difference between (**c**) and (**a**)

moisture flux reduces over land with the exception of a few locations at the north (Fig. 7e). There exists a dipole of induced changes in moisture flux with negative pole at the north (centred 15°N) and positive pole at the south (centred 5°N) based on the TSI + 5 W m^{-2} experiment and vice versa (Fig. 7d, e). The moisture flux increase in the TSI + 5 W m^{-2} experiment can be explained based on evaporation and transpiration increase which increases the moisture in the atmosphere. The reverse is the case with the TSIT – 5 W m^{-2} experiment. The dipole change structure of vertically integrated meridional moisture flux reverses direction based on moisture availability through the effect of TSI changes (Fig. 7d, e). Figure 8 shows simulated evaporation in the three experiments and the difference between TSI ± 5 W m^{-2} and control experiments. Evaporation is normally high on the ocean and southern part of the simulation domain due to the presence of water bodies and vegetation. Evapotranspiration

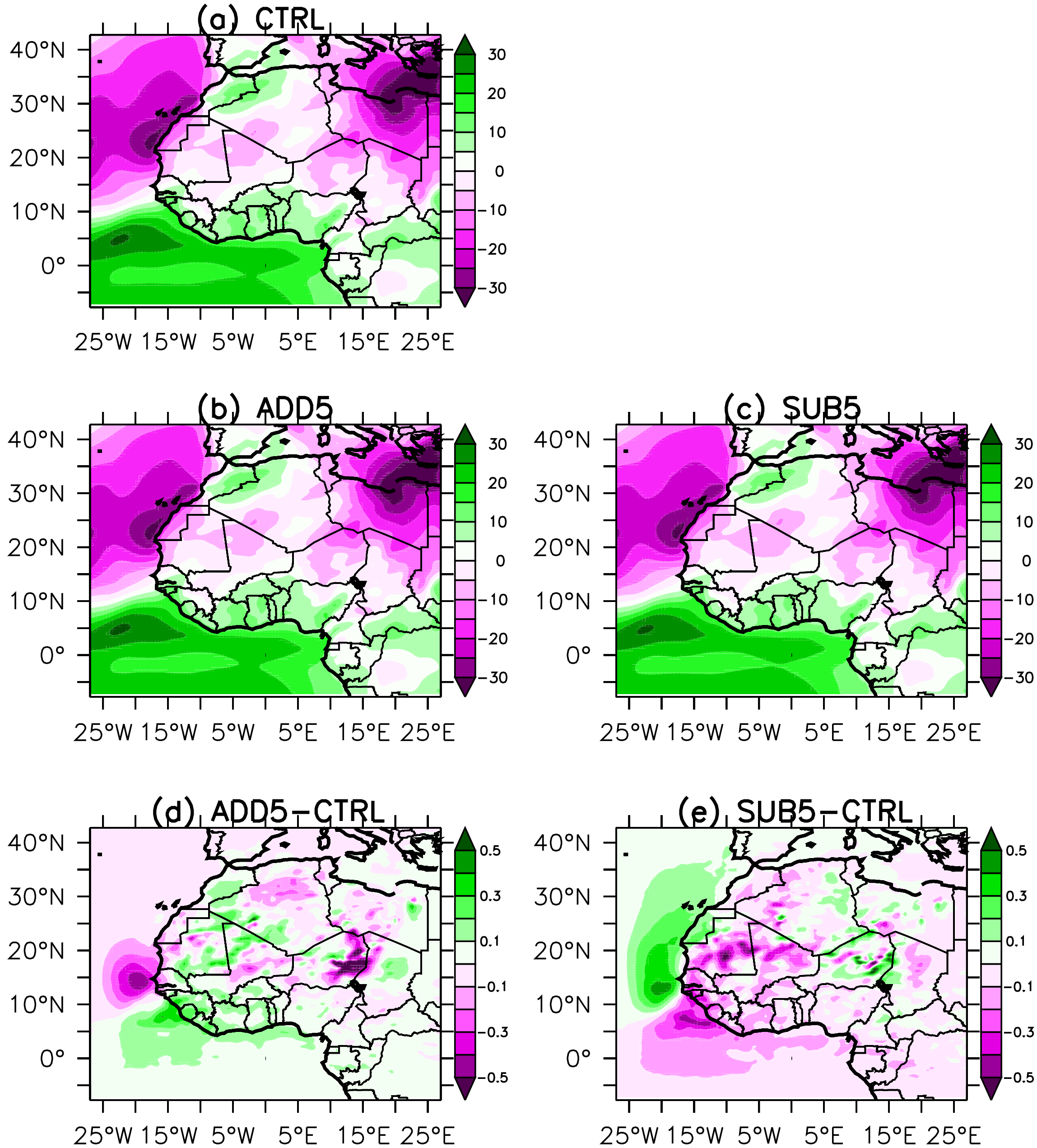

Fig. 7 Mean JJAS integrated meridional moisture flux from 1000 to 300 hpa in **a** control simulation, **b** TSI + 5 W m^{-2} experiment, **c** TSI − 5 W m^{-2} experiment, **d** difference between (**b**) and (**a**), and **e** difference between (**c**) and (**a**)

increases generally with TSI increase over the ocean and strongly between 15 and 20°N on land, while it reduces on the ocean and strongly between 15 and 25°N on land with the TSI − 5 W m^{-2} experiment. However, there are patches of opposite induced changes (Fig. 8d, e). The evapotranspiration increase with TSI increase supports the increase in moisture flux in TSI + 5 W m^{-2} experiment and vice versa (Figs. 7d, e, 8d, e). Figure 9 shows the simulated difference between potential evapotranspiration (PET) and actual evapotranspiration (ET) (PETET) and the changes induced by TSI ± 5 W m^{-2}. This parameter is an indication of excess water requirement by vegetation which should be supplied in form of irrigation. Normally, the need for irrigation at the southern countries is very low, while it is high at the northern countries (Fig. 9a). Increase in TSI generally increases moisture flux (Fig. 7d), evapotranspiration (Fig. 8d), and precipitation (Fig. 5d), especially at the south. It has little effect on PETET at the south, but reduces PETET noticeably between 15 and 25°N. However, there are patches of increased PETET between 25

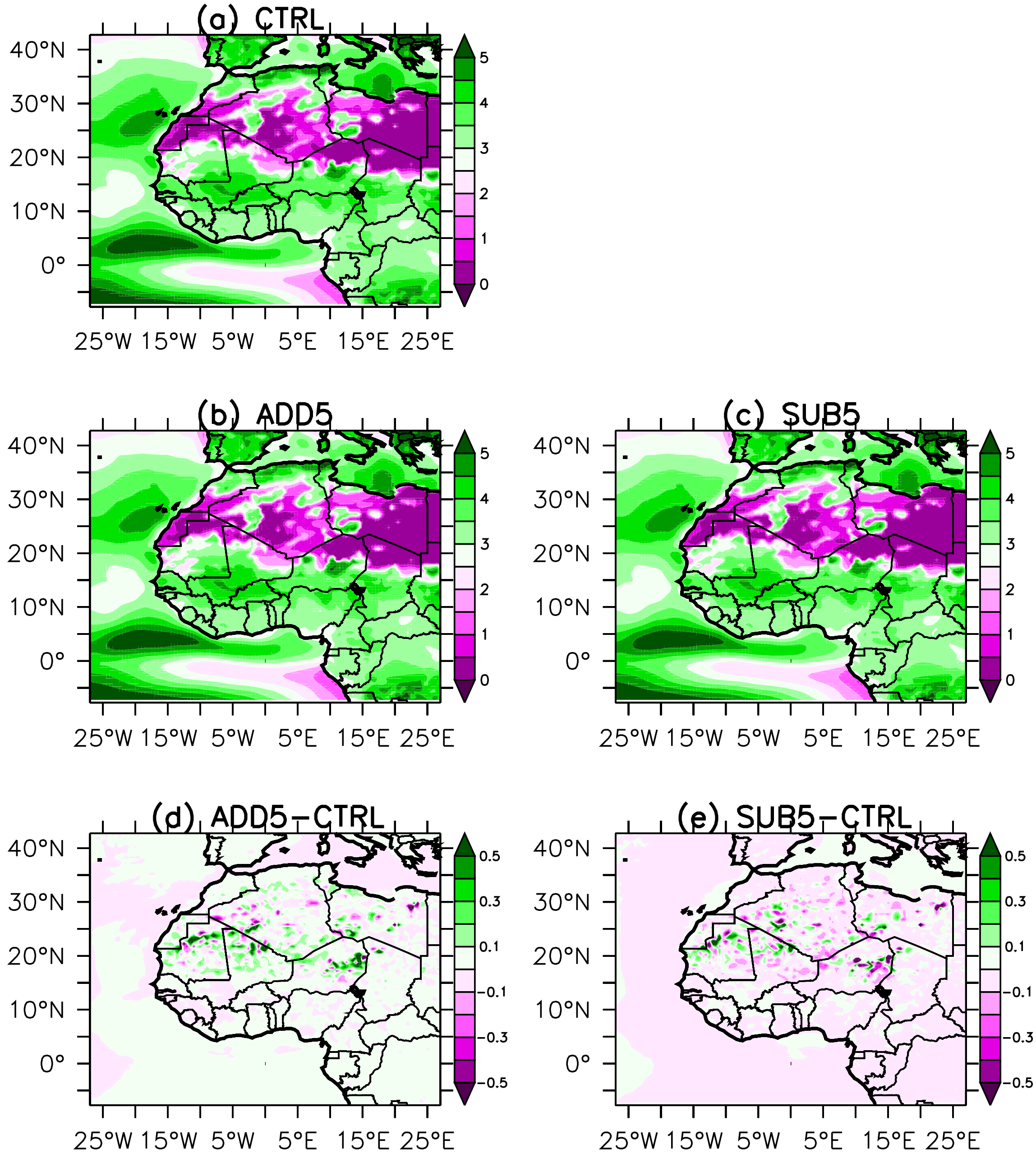

Fig. 8 Mean JJAS actual evapotranspiration in **a** control simulation, **b** TSI + 5 W m^{-2} experiment, **c** TSI − 5 W m^{-2} experiment, **d** difference between (**b**) and (**a**), and **e** difference between (**c**) and (**a**)

and 30°N. Reduction in TSI has little effect on PETET at the southern area of the simulation domain, but leads to noticeable increase in PETET at the north from latitude 15°N and above. However, there exist patches of reduced PETET probably due to the presence of small water bodies in those areas. This is because opposite induced effects of TSI changes on PETET are associated with land and ocean (Fig. 9d, e).

4.7 Induced Changes in Mean Seasonal Comfort Index Based on Changes in TSI

Simulated mean seasonal comfort index and induced changes in the index associated with TSI ± 5 W m^{-2} changes are shown in Fig. 10. The DI on land is generally above 72 with the exception of a few locations where it is between 68 and

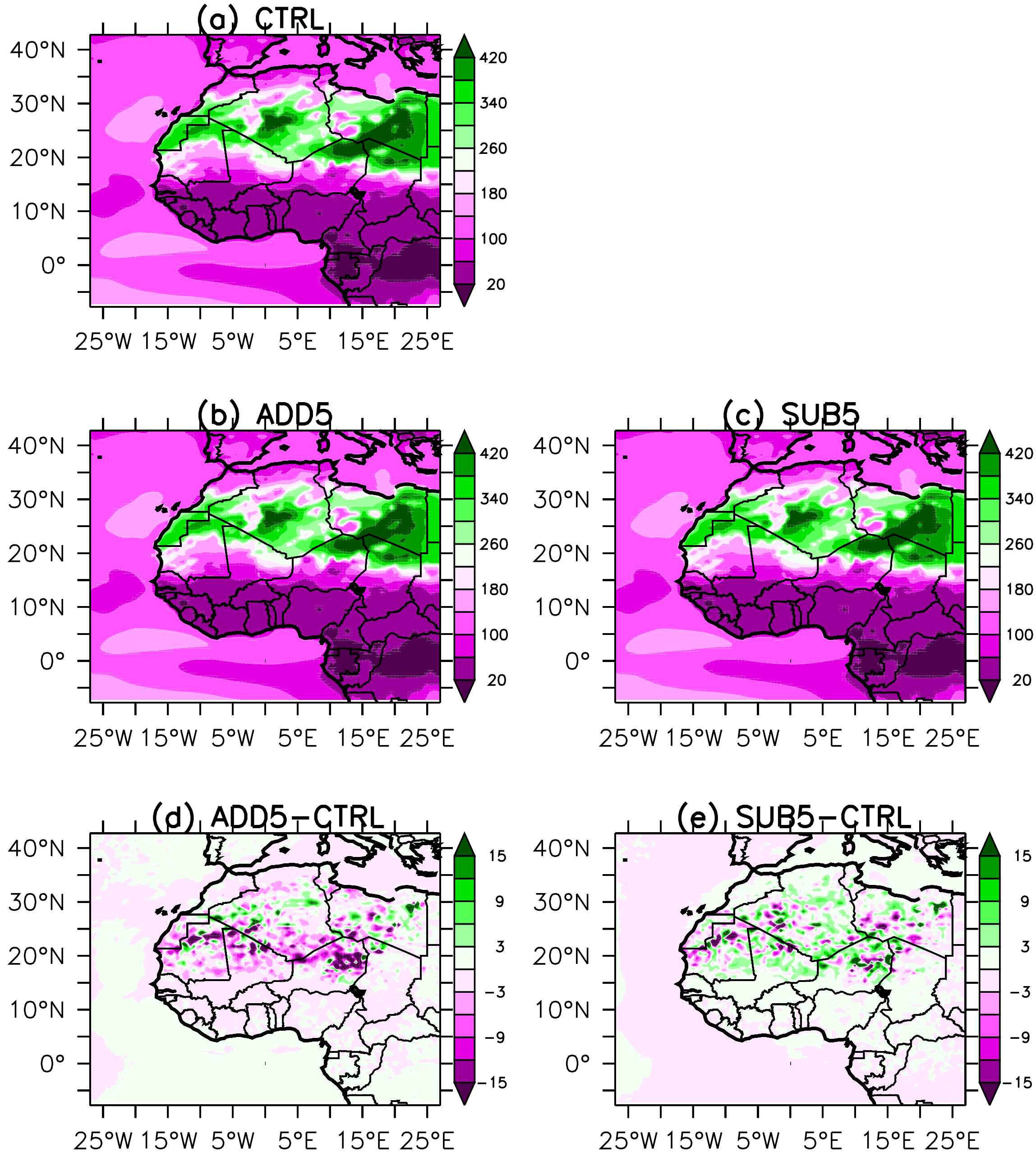

Fig. 9 Mean JJAS difference between potential evapotranspiration and actual evapotranspiration in **a** control simulation, **b** TSI + 5 W m^{-2} experiment, **c** TSI − 5 W m^{-2} experiment, **d** difference between (**b**) and (**a**), and **e** difference between (**c**) and (**a**)

72 (Fig. 10a). No cold-related discomfort is simulated on land with control TSI. The whole population in the simulation domain is generally comfortable in most places on land except for 12–30°N at the west and some locations at the east and central parts where DI is greater than 75. With increase in TSI, DI slightly increases generally and vice versa except for a few locations (eastern Niger and surroundings) (Fig. 10d, e). The reduction/increase in DI at Niger and its environs is attributable to the evaporative cooling in the area with TSI increase and vice versa (Fig. 8d, e). The border DI values have the potential to reach uncomfortable level with TSI increase, but, with TSI reduction, the normal comfortable level could be maintained.

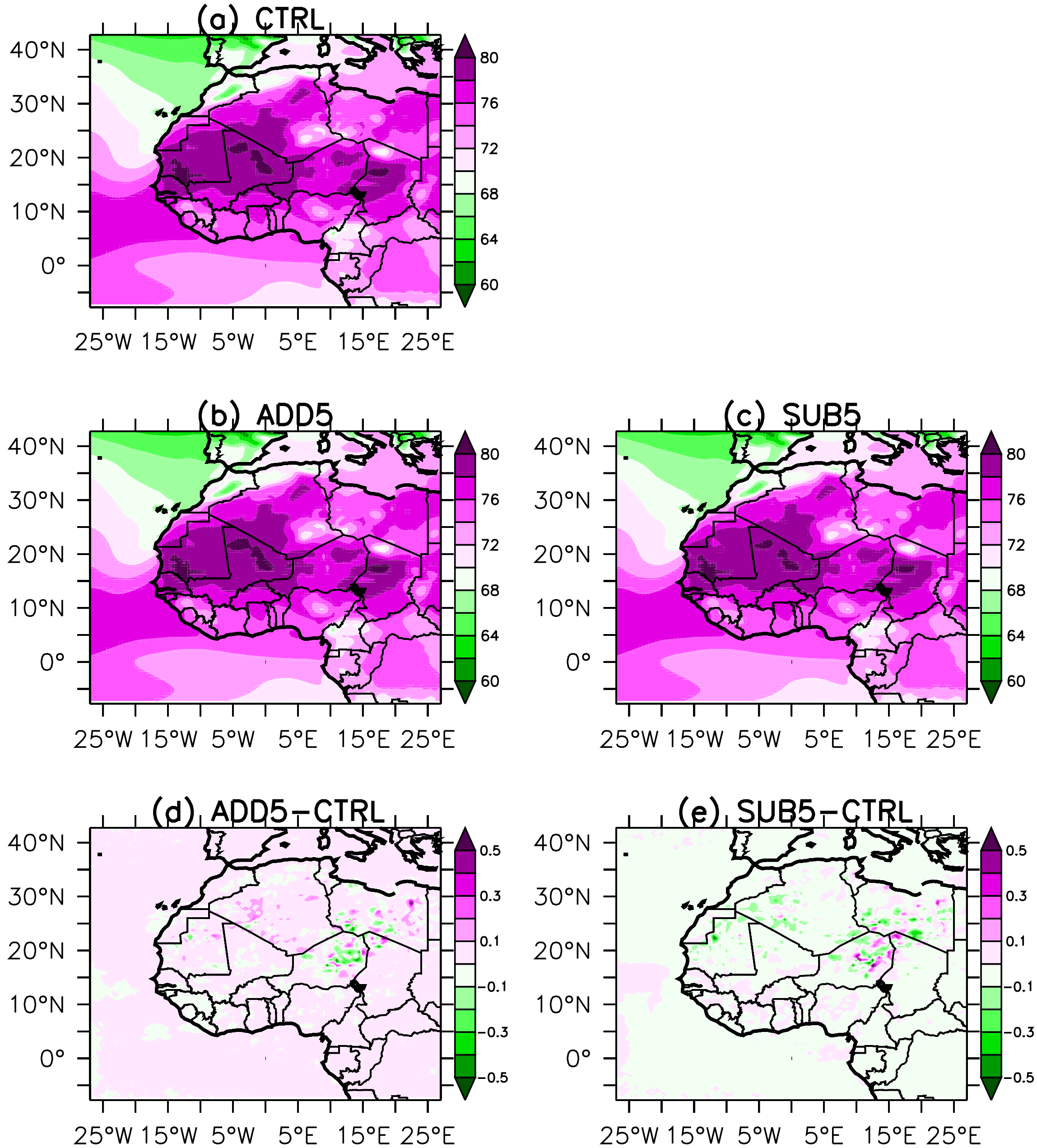

Fig. 10 Mean JJAS discomfort index in **a** control simulation, **b** TSI + 5 W m^{-2} experiment, **c** TSI – 5 W m^{-2} experiment, **d** difference between (**b**) and (**a**), and **e** difference between (**c**) and (**a**)

5 Conclusion

RegCM4.7 fairly captures the diurnal precipitation trend, intra-annual variations of precipitation, and temperature over West Africa. However, there are biases which are predominantly negative except at WWA. The effect of variations in TSI on the climate of West Africa depends on latitude, presence of vegetation, and water bodies. Increase in TSI generally increases evaporation, moisture flux, and precipitation except for reduction in some places. It also increases temperature except at latitudes 15–25°N, where temperature reduces strongly, probably due to evaporative cooling. TSI reduction results in exactly opposite effect. A dipole change structure in moisture flux with positive centred at ~ 7°N and negative ~ 15°N is simulated in TSI +5 W m^{-2} experiment. A similar dipole with reversed sign is found with the TSI – 5 W m^{-2} experiment. The lower southwestern area of the simulation domain (Guinea, Sierra Leone, and Liberia) show contrary temperature changes for both TSI increase and reduction. This can be attributed to the location of positive and negative poles of integrated meridional moisture flux at the area in the TSI + 5 W m^{-2} and TSI − 5 W m^{-2} experiment, respectively. The positive pole with increased moisture flux reduces temperature, while the negative flux with reduced moisture flux results in increased temperature at the area.

Demand for irrigation is simulated to reduce in the TSI + 5 W m^{-2} experiment, while it increases in TSI − 5 W m^{-2} experiment. Latitudes 21–30°N in TSI + 5 W m^{-2} experiment show the patches of contradictory response compared to other areas. There are also patches of contrary response in the TSI − 5 W m^{-2} experiment. The contrary response is attributed to presence of some water bodies in those locations. In general, irrigation needs increase and decrease on the ocean for the TSI + 5 W m^{-2} and TSI − 5 W m^{-2}, respectively. Normally irrigation is not considered over ocean, but it explains the contrary response on lands that have some water bodies located on them. Discomfort index increases with increased TSI, while it reduces with reduced TSI. The number of uncomfortable people will increase with increased TSI, while reduced TSI is not going to change the comfort level of the population. Significant TSI variations coupled with some other changes that affect climate such as increase in the levels of greenhouse gases may have serious implication on water resources, agricultural productivity, and health of the West African population.

Acknowledgements This work was carried out at the Abdus Salam International Centre for Theoretical Physics. All the facilities used were fully provided by the Centre. The monthly precipitation and temperature data used for model validation are partly obtained from the NOAA/OAR/ESRL PSD, Boulder, CO, USA, from their Web site at https://www.esrl.noaa.gov/psd/. The CRU data are used in this study which is provided by Climate Research Unit of the University of East Anglia. The author is grateful to the UCAR NCAR for releasing the TRMM_3B42 data.

Compliance with Ethical Standards

Conflict of Interest The author states that there is no conflict of interest.

References

Adeniyi MO (2009) Determination of heat stress in the tropical urban area of Ibadan, Southwestern Nigeria. Int J Nat Appl Sci 5(3):235–243

Adeniyi MO (2014) Sensitivity of different convection schemes in RegCM4.0 for simulation of precipitation during the Septembers of 1989 and 1998 over West Africa. Theor Appl Climatol 115(1–2):305–322. https://doi.org/10.1007/s00704-013-0881-5

Adeniyi MO (2016) The consequences of the IPCC AR5 RCPs 4.5 and 8.5 climate change scenarios on precipitation in West Africa. Clim Change 139:245–263. https://doi.org/10.1007/s10584-016-1774-2

Adeniyi MO (2017) Modeling the impact of changes in Atlantic sea surface temperature on the climate of West Africa. Meteorol Atmos Phys 129:187–210. https://doi.org/10.1007/s00703-016-0473-x

Adeniyi MO, Oyekola SO (2017) Assessment of heat and cold wave events over West Africa using three regional climate models. Ann Geophys 60(3):A0322. https://doi.org/10.4401/ag-7039

Adeniyi MO, Nymphas EF, Oladiran EO (2012) Characteristics of total solar radiation in an urban tropical environment. Int J Phys Sci 7(30):5154–5161. https://doi.org/10.5897/IJPS09.253

Akisanola AA, Ogunjobi KO, Ajayi VO, Adefisan EA, Omotosho JA, Sanogo S (2016) Comparison of five gridded precipitation products at climatological scales over West Africa. Meteorol Atmos Phys. https://doi.org/10.1007/s00703-016-0493-6

Bassham JA, Hans LH (2018). Photosynthesis encyclopædia britannica encyclopædia britannica, Inc. https://www.britannica.com/science/photosynthesis. Accessed 09 July 2018

Ben Salem M, Bouraoui R (2009) Heat stress in Tunisia: effects on dairy cows and potential means of alleviating it. S Afr J Anim Sci 39:256–259

Bermejo R, Staniforth A (1992) The conversion of semi-Lagrangian advection schemes to quasi-monotone schemes. Mon Wea Rev 120:2622–2632

Chafa MC (2015) Temporal variation of temperature and relative humidity and the responses by the Friesian × Bunaji cross breed cows in Shika Zaria, Kaduna State, Nigeria. M.Sc. Dissertation. Ahmadu Bello University, Zaria

Coppola E, Giorgi F, Raffaele F, Fuentes-Franco R, Giuliani G, LLopart-Pereira M, Mamgain A, Mariotti L, Diro GT, Torma C (2014) Present and future climatologies in the phase I CREMA experiment. Clim Change 125(1):23–38. https://doi.org/10.1007/s10584-014-1137-9

Dee DP, Uppala SM, Simmons AJ, Berrisford P, Poli P, Kobayashi S, Andrae U, Balmaseda MA, Balsamo G, Bauer P, Bechtold P, Beljaars ACM, van de Berg L, Bidlot J, Bormann N, Delsol C, Dragani R, Fuentes M, Geer AJ, Haimberger L, Healy SB, Hersbach H, Hólm EV, Isaksen L, Kållberg P, Köhler M, Matricardi M, McNally AP, Monge-Sanz BM, Morcrette J-J, Park B-K, Peubey C, de Rosnay P, Tavolato C, Thépaut J-N, d Vitart F (2011) The ERA-interim reanalysis: configuration and performance of the data assimilation system. Quart J R Meteorol Soc 137:553–597. https://doi.org/10.1002/qj.828

Du Preez JH, Giesecke WH, Hahingh PJ (1990) Heat stress in dairy cattle and other livestock under southern African conditions temperature–humidity index mean values during the four main seasons. Onderstepoort J Vet Res 57:77–87

Espenak F (1989) Fifty year canon of lunar eclipses: 1986–2035. Sky Publishing Corporation, Cambridge, MA

Gantner V, Mijić P, Kuterovac K, Solić D, Gantner R (2011) Temperature–humidity index values and their significance on the daily production of dairy cattle. Mljekarstvo 61(1):56–63

Gao X, Shi Y, Giorgi F (2016) Comparison of convective parameterizations in RegCM4 experiments over China with CLM as the land surface model. Atmos Ocean Sci Lett 9(4):246–254. https://doi.org/10.1080/16742834.2016.1172938

Giorgi F, Coppola E, Solmon F, Mariotti L, Sylla MB, Bi X, Elguindi N, Diro GT, Nair V, Giuliani G, Turuncoglu UU, Cozzini S, Güttler I, O'Brien TA, Tawfik AB, Shalaby A, Zakey AS, Steiner AL, Stordal F, Sloan LC, Brankovic C (2012) RegCM4 model description and preliminary tests over multiple CORDEX domains. Clim Res 52:7–29. https://doi.org/10.3354/cr01018

Guo A, Moore JC, Ji D (2018) Tropical atmospheric circulation response to the G1 sunshade geoengineering radiative forcing experiment. Atmos Chem Phys 18:8689–8706. https://doi.org/10.5194/acp-18-8689-2018

Harris I, Jones PD, Osborn TJ, Lister DH (2014) Updated high-resolution grids of monthly climatic observations in the CRU TS3.10 dataset. Int J Climatol 34:623–642. https://doi.org/10.1002/joc.3711

Hostetler SW, Bates GT, Giorgi F (1993) Interactive coupling of a lake thermal model with a regional climate model. J Geophys Res 98:5045–5057. https://doi.org/10.1029/92JD02843

Huffman GJ, Adler RF, Bolvin DT, Gu G, Nelkin EJ, Bowman KP, Hong Y, Stocker EF, Wolff DB (2007) The TRMM multi-satellite precipitation analysis: quasi-global, multi-year, combined-sensor precipitation estimates at fine scale. J Hydrometeor 8:38–55

Kain JS (2004) The Kain–Fritsch convective parameterization: an update. J Appl Meteorol 43:170–181

Kain JS, Fritsch JM (1990) A one-dimensional entraining/detraining plume model and its application in convective parameterization. J Atmos Sci 47:2784–2802

Kibler HH (1964). Thermal effects of various temperature–humidity combinations on Holstein cattle as measured by eight physiological responses. Missouri agricultural experiment, Exp. Stn Res Bull 862, Mt Vernon. Environmental Physiology and Shelter Engineering, LXVII

Kopp G (2016) Magnitudes and timescales of TSI variability. JSWSC. https://doi.org/10.1051/swsc/2016025

Legates DR, Willmott CJ (1990) Mean seasonal and spatial variability in gauge-corrected, global precipitation. Int J Climatol 10:111–127

Lithman M, Espenak F (2017) Totality: the great American eclipse of 2017 and 2024, 1st edn. Oxford University Press, New York

Miguez-Macho G, Stenchikov GL, Robock A (2005) regional climate simulations over North America: interaction of local processes with improved large-scale flow. J Clim 18:1227–1246. https://doi.org/10.1175/JCLI3369.1

Montheith JL, Unsworth MH (2013) Principles of environmental physics, plants, animals and the atmosphere, 4th edn. Academic Press, UK

Nymphas EF, Adeniyi MO, Oladiran EO (2009) Micrometeorological measurement in Nigeria during the total solar eclipse of 29 Mar 2006. J Sol Terr Phys 71:1245–1253

Okpara JN, Kolawole SM, Gbuyiro SO, Okwara MO (2002) Investigating the effects of weather parameters on the human comfort and discomfort of inhabitants of urban environments of Akure, in Nigeria. J Niger Meteorol Soc 3(3):12–18

Philander SG (1998) Is the temperature rising? The uncertain science of global warming. Princeton University Press, Princeton

Rojas M (2006) Multiply nested regional climate simulation for southern South America: sensitivity to model resolution. Mon Weather Rev 134:2208–2223

Soares WR, Marengo JA (2009) Assessments of moisture fluxes east of the Andes in South America in a global warming scenario. Int J Climatol 29:395–1414

Thom EC (1959) The discomfort index. Weatherwise 12:57–59

Tietdke M (1996) An extension of cloud-radiation parameterization in the ECMWF model: the representation of subgrid-scale variations of optical depth. Mon Weather Rev 124:745–750

Tsukernik M, Lynch AH (2013) Atmospheric meridional moisture flux over the southern ocean: a story of the Amundsen Sea. J Clim 26:8055–8064

Wild M (2009) Global dimming and brightening: a review. J Geophys Res 114:D00D16. https://doi.org/10.1029/2008JD011470

Willmott CJ, Matsuura K (1995) Smart interpolation of annually averaged air temperature in the United States. J Appl Meteorol 34:2577–2586

Willmott CJ, Matsuura K (2001) Terrestrial air temperature and precipitation: monthly and annual time series (1950–1999). http://climate.geog.udel.edu/~climate/html_pages/README.ghcn_ts2.html. Accessed 12 June 2018

Yeo KL, Krivova NA, Solanki SK, Glassmeier KH (2014) Reconstruction of total and spectral solar irradiance from 1974 to 2013 based on KPVT, SoHO/MDI, and SDO/HMI observations. A&A 570:A85. https://doi.org/10.1051/0004-6361/201423628

Zaehle S, Ciais P, Friend AD, Prieur V (2011) Carbon benefits of anthropogenic reactive nitrogen offset by nitrous oxide emissions. Nat Geosci 4(9):601–605

Zhang H, Bai X, Xue J, Chen Z, Tang H, Chen F (2013) Emission of CH4 and N2O under different tillage systems from double-cropped paddy fields in southern China. PLoS One 8(6):e65277. https://doi.org/10.1371/journal.pone.0065277